Improvement of the photocatalytic performance of ZnO thin films in the UV and sunlight range by Cu doping and additional coupling with Cu2O

F.Z. Nouasria, D. Selloum, A. Henni, Sophie Tingry, J. Hrbac

Improvement of the photocatalytic performance of ZnO thin films in the UV and sunlight range by Cu doping and additional coupling with Cu_2O

F. Z. Nouasria[a], D. Selloum[a*], A. Henni[a], S. Tingry[b], J. Hrbac[c]

[a] *Lab. Dynamic Interactions and Reactivity of Systems, Kasdi Merbah University, Ouargla, 30000, Algeria*

[b] *Institut Européen des Membranes, UMR 5635, Université Montpellier, ENSCM, CNRS, Montpellier, France*

[c] *Institute of Chemistry, Masaryk University, Kamenice 5, Brno 62500, Czech Republic*

*** Corresponding Author** -mail: selloumdjamel@gmail.com, selloum.djamel@univ-ouargla.dz

(Djamel Selloum)

Abstract

Thin films of ZnO, Cu-doped ZnO, Cu_2O and binary Cu_2O/Cu-doped ZnO p-n heterojunction thin film were prepared and tested for their heterogeneous photocatalytic activity in the removal of three selected organic dyes: methylene blue (MB), methylene orange (MO) and Congo red (CR). The photocatalytic experiments were carried out under UV light and natural sunlight. The synthesis of the thin film photocatalysts was carried out by an electrochemical deposition method and the resulting films were characterized by scanning electron microscope (SEM), X-ray diffraction (XRD), UV-Vis spectroscopy, electrochemical impedance spectroscopy and capacitance measurements (i.e., Mott-Schottky plots). Under UV illumination, the results showed that the photocatalytic degradation activity is of first-order kinetics and the lifetime of the photogenerated electron-hole pairs of ZnO is increased by the Cu doping. The combination of Cu-doped ZnO and Cu_2O allows the construction of a p-n heterojunction that enhances the photocatalytic process, as demonstrated for the photocatalytic degradation of dyes under sunlight irradiation.

Key words: Thin films; Heterojunction; Electrodeposition; Photocatalysis; Sunlight irradiation; organic dyes.

Graphical abstract

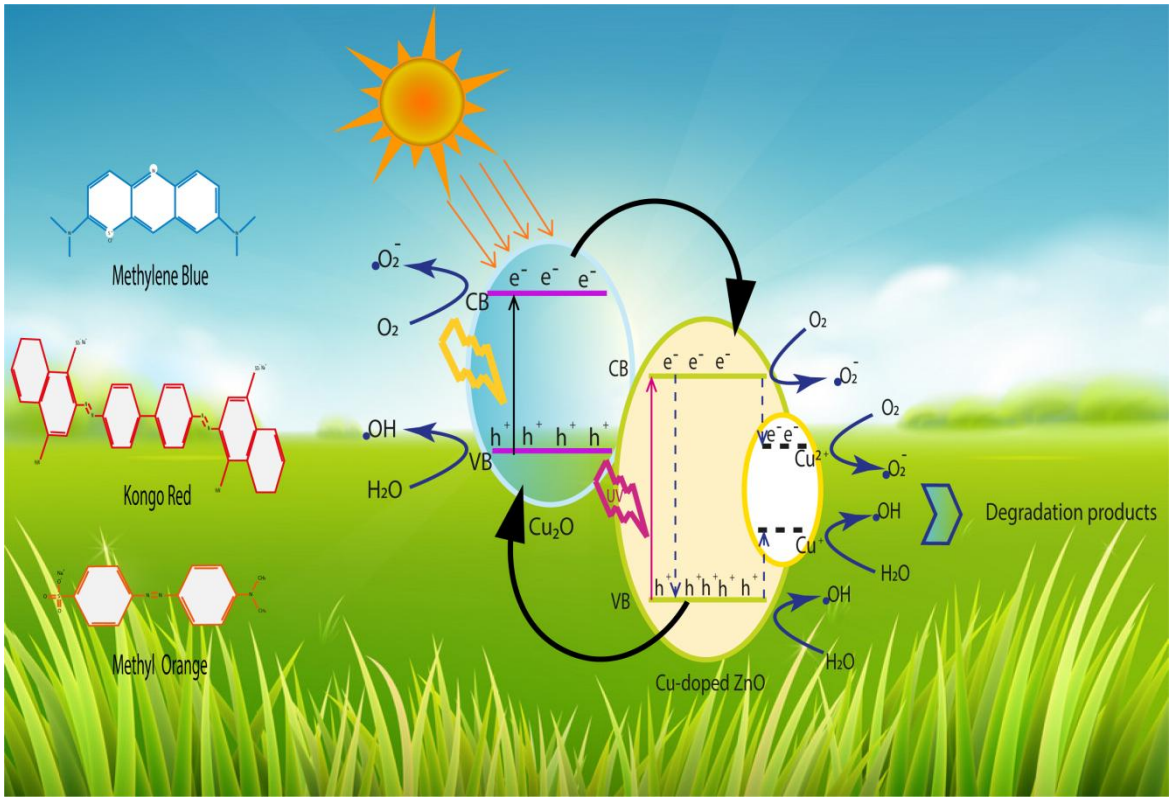

1. Introduction

The technological development that has occurred in recent years in various fields such as electronics, optoelectronics, environment and photovoltaics, has led to new avenues of research aimed at developing low-cost materials with controlled electrical and optical properties. Metal oxide semiconductors have shown significant promise for a variety of practical applications. In particular, the materials ZnO and Cu_2O have attracted the attention of researchers in various fields, as they are abundant and cheap to manufacture, meet the requirements of clean renewable energy and cost-efficient fabrication, and exhibit good optoelectronic properties [1–4]. Recently, Cu_2O and ZnO have attracted interest in the development of new technologies for wastewater treatment [5–9]. In the field of wastewater treatment, the main source of water pollution is the uncontrolled discharge of industrial effluents from various operations, including the manufacturing, printing, food and textile industries [10]. In particular, the world produces about $8 \cdot 10^5$ tons of synthetic dyes each year, which are mainly used in the food, textile and beauty industries due to their wide range of colors and chemical stability [11].

Approximately 10-15% of these non-biodegradable textile dyes are lost to the surrounding freshwater systems during the manufacturing and application processes [12]. Advanced oxidation processes (AOPs) are one of the most advanced methods for treating organic-polluted water. The advantage of this technique is the possibility to remove organic products, such as pesticides and dyes, which cannot be treated by other conventional methods due to their high chemical stability and low biodegradability [13,14]. The most common processes are :(i) UV/O_3, which is limited by the low solubility of O_3 in water and high energy costs for ozone generation, (ii) UV/H_2O_2 which has low absorption to UV radiation, reducing degradation efficiency and potential production of bromine as aby-product [11,15], and (iii) the Fenton reaction which generates iron sludge as a by-product and operates at low pH increasing the operation cost.

Due to these limitations, the process of heterogeneous photocatalysis is a promising method based on radiations to photo-excite a semiconductor catalyst. When a semiconductor is hit by a photon of energy greater than or equal to its bandgap energy, an electron (e^-) is released to move from the valence band to the conduction band (CB), leaving an unoccupied site as a hole (h^+) in the valence band (VB). The (e^-, h^+) pairs formed generate strong oxidizing radicals such as hydroxyl (•OH) and superoxide ($\bullet O_2^-$) radicals that can breakdown organic substances and make them harmless [16]. The process of photocatalytic activity is determined

by two factors: the harvesting of a large number of photons and the effective separation of the photogenerated electron-hole pairs. Photons absorption is highly dependent on the bandgap structure of the semiconductor; however, the majority of currently available stable photocatalysts have a large bandgap, which limits their light absorption spectrum. Only the photoexcited electrons and holes that reach the surface of the semiconductor photocatalyst contribute to the photocatalytic process, while the majority are easily recombined [17]. In this regard, various approaches have been proposed to significantly enhance light absorption and reduce recombination of photoexcited electron-hole pairs of the photocatalyst. Doping the bulk photocatalyst adds extra energy levels in the bandgap, which helps to effectively separate charge carriers by trapping photogenerated electrons or holes, allowing more of them to diffuse to the surface [18–20]. The combination of two semiconductors forming a hybrid photocatalyst, where electrons are transferred to the CB of one semiconductor and holes to the VB of the other semiconductor at the interface, prevents charge recombination [21]. Most studies refer to the use of Cu_2O/ZnO heterostructure films as hybrid photocatalysts in photovoltaic devices [22–24]. In addition, both techniques can exploit solar energy conversion by extending the absorption ability of the semiconductors to the visible region. In addition, the use of thin-film rather than powdered photocatalysts is a convenient way to avoid the extra procedures related to the separation and recovery processes of the reaction mixture [25]. The most commonly used methods for the development of thin-films photocatalysts are not only complicated and involve expensive processing, but also use high temperature processing. In contrast, the electrochemical electrodeposition technique (ECD) has a number of attractive features, such as the use of a relatively low processing temperature, low-cost, direct control of deposition conditions as well as electrolyte composition, simplicity and safety of the process, and the potential for large-scale production. To our knowledge there is no work on the electrodeposition of Cu_2O/ZnO thin films using a fully electrochemical approach for photocatalytic applications.

This study therefore focuses on the removal of Methylene blue (MB), Methyl orange (MO) and Congo red (CR) dyes, by heterogeneous photocatalysis with the aim of extending the lifetime of the photogenerated electron-hole pairs of the semiconductor ZnO by Cu doping. In order to eliminate costly artificial light sources, the photocatalytic degradation of the dyes was achieved by natural sunlight irradiation, which is an abundant, environmentally friendly and renewable energy source.

2. Experimental

2.1 Photocatalysts synthesis

2.1.1 Synthesis of ZnO and Cu-doped ZnO

A conventional three-electrode cell, with a saturated calomel electrode (SCE) was used as a reference electrode, a Pt foil as auxiliary and the ITO glass substrate (geometric area 1 cm^2) as the working electrode was used for the electrodeposition of the photocatalysts. The electrodeposition was performed using a PGSTAT204 potentiostat/galvanostat (Metrohm Autolab, Switzerland). The ZnO photocatalysts were deposited on ITO by electrodeposition of a 0.1 M KCl, 5 mM $ZnCl_2$ and 5 mM H_2O_2 solution, maintained at 70 °C. The applied potential was -1.0 V vs. SCE for 40 min. The Cu-doped ZnO photocatalysts were deposited in the same bath in which copper (II) chloride ($CuCl_2$) was added as the dopant precursor. The molar concentration ratio [$CuCl_2$]/[$ZnCl_2$] was set at 0.5%, according to our previous research work to obtain the best performance in terms of photocurrent generation [26]. Freshly synthesized films were washed with deionized water and dried in air.

2.1.2 Synthesis of Cu_2O

Cuprous oxide (Cu_2O) photocatalysts were prepared using the same method as for the electrodeposition of pure and Cu-doped ZnO. The deposition solution contained 5×10^{-2} M of $CuSO_4$ and 5×10^{-2} M of citric acid ($C_6H_8O_7$). The pH of the solution was adjusted to 12.5 with NaOH in order to deposit p-type Cu_2O [27]. The applied potential was -0.5 V vs. SCE for 60 min at 65 °C. After deposition, the films were washed with deionized water and dried in ambient air.

2.1.2 Synthesis of Cu_2O/ZnO heterostructure

The synthesis of Cu_2O/ZnO photocatalysts was carried out using layer-by-layer deposition. The first layer was ZnO or 0.5% Cu-doped ZnO, followed by a second layer of Cu_2O thin film. All layers were successively electrodeposited under the same conditions as described above.

2.2 Characterization

The synthesized photocatalysts were characterized by imaging and physico-chemical techniques. For the observation of the surface morphology, scanning electron microscope (JEOL JSM-7001F) was used. For the identification of the phase/structure of the thin films,

XRD analysis was performed with a Bruker AXS D8 Advance X-ray diffractometer with Cu-K_α radiation (λ=1.54 Å). The absorbance and transmittance data of the films were recorded with a UV-2300 (Shimadzu) spectrophotometer. The electrochemical impedance spectroscopy (EIS) and Mott-Schottky (MS) analysis were performed in 0.1 M Na_2SO_4 solution in the dark. The EIS measurements were registered in the range (100 kHz – 10^{-1} Hz) at the open circuit potential. Mott-Schottky (MS) analysis was carried out in the potential range from -1 to 1 V at an amplitude of 0.01 V, and a frequency of 200 Hz and 1000 Hz for ZnO and Cu_2O, respectively. Chemical state was determined by photoelectron spectroscopy (XPS) analysis using (Kratos Axis Ultra) and analyzed using CASA software.

2.3 Photocatalysis experimental protocol

Two different tests of the photocatalytic performance of the photocatalysts were performed.
The first test was carried out under UV irradiation. ZnO and Cu-doped ZnO thin film photocatalysts were added to beakers, each containing a fixed volume of 25 mL of aqueous solution containing the three dyes methylene blue (MB), methyl orange (MO) and Congo red (CR) at the concentration of 10 μM. The mixtures were irradiated in a chamber containing four UV lamps (365 nm) with a total power of 30 W. The second test was carried out under natural sunlight for Cu-doped ZnO, Cu_2O, and Cu-doped ZnO/Cu_2O thin film photocatalysts. The same conditions were used to investigate the effect of sunlight as an excitation source for the photocatalysts. The power intensity of sunlight was measured by solarimeter (SL 200 - KIMO) every half-hour and found to be 700–900 W/m^2 (the experiments were carried out in April 2021). The photocatalytic degradation process was monitored by a UV-Vis spectrophotometer by recording the absorption spectra every half-hour to control the change in dyes concentration with the time. The degradation efficiency was defined as follow:

$$D = \frac{A - A_t}{A} \times 100 \quad (1)$$

where A and A_t are the values of the initial absorbance and absorbance at the actual measurement time, respectively, at λ_{max} (660 nm for MB, 464 nm for MO and 500 nm for CR).

3. Results and discussion

3.1. SEM/EDS observations

The SEM images of the surface morphologies of the synthesized ZnO, Cu-doped ZnO, Cu_2O and Cu_2O/Cu-doped ZnO films are presented in Fig. 1. In the absence of Cu^{2+} ions, the surface of ZnO appears as a flat surface consisting of uniformly arranged and closely packed hexagonal nanorods (Fig. 1a). However, the nanorods become smaller with the inclusion of Cu atoms in the ZnO lattice and other structures begin to appear (Fig. 1b). The Cu_2O surface (Fig. 1c) shows a triangular prism and pyramid morphology with sharp edges and corners that cover the surfaces uniformly. The combination of Cu_2O and Cu-doped ZnO (Fig. 1d) shows that the Cu_2O thin film successfully covers the entire surface of the ZnO nanorods where some of the deposited crystals are hexagonal pyramids, suggesting that the hexagonal ZnO nanorods act as nucleation sites for Cu_2O growth.

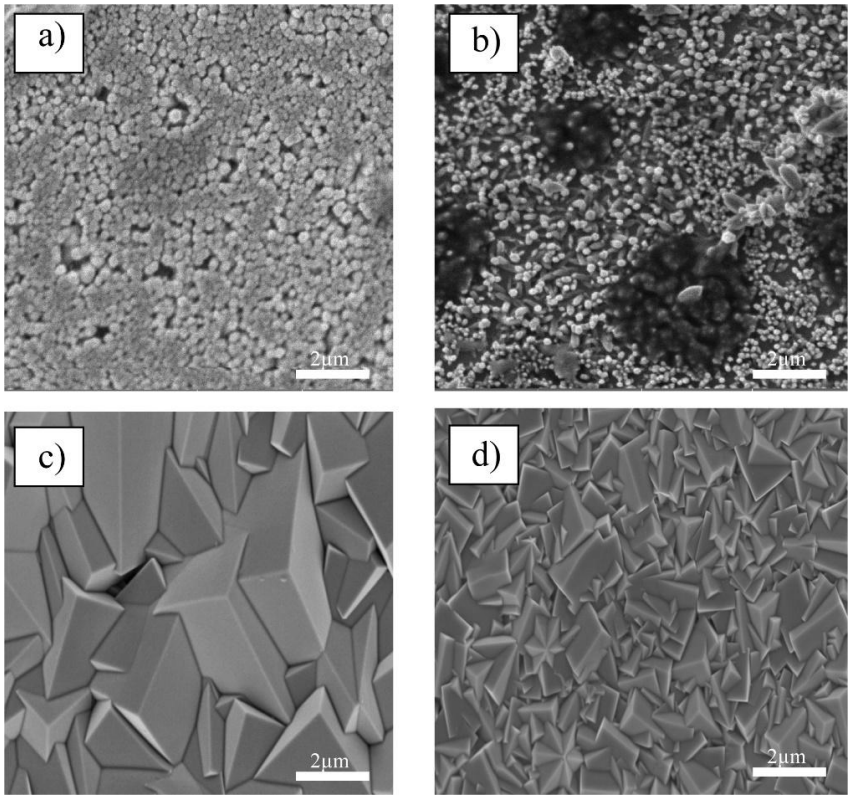

Fig. 1. SEM photographs for: **a)** ZnO, **b)** Cu-doped ZnO, **c)** Cu_2O and **d)** Cu_2O/Cu-doped ZnO.

The Cu content in the deposits determined by Energy dispersive spectroscopy (EDS) measurements are shown in fig. 2 and point to the presence of Zn and O for pure ZnO while the Zn, O, and Cu elements for the doped samples reveal the successful incorporation of Cu in the ZnO lattice.

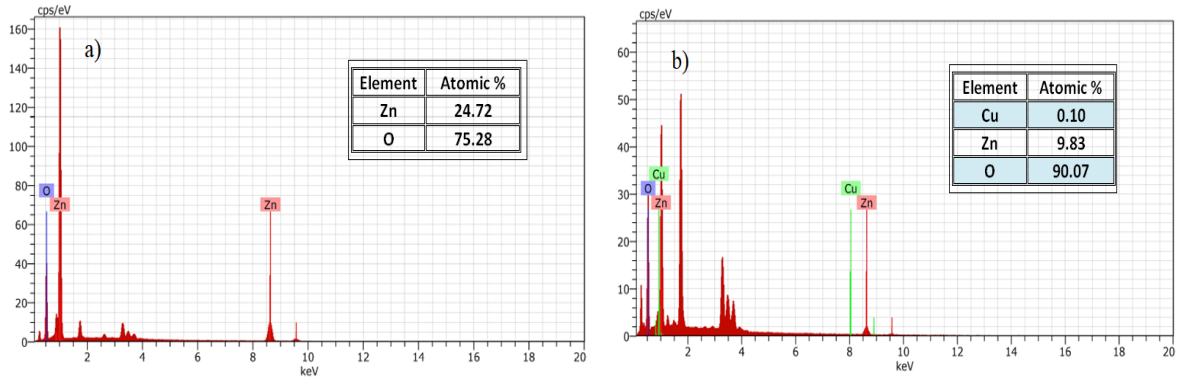

Fig. 2. EDS spectrum obtained for: **a)** ZnO, **b)** Cu-doped ZnO.

3.2. XRD analysis

To investigate the crystal phase/structure and orientation of the as-prepared photocatalysts, XRD analyses were performed and the results are shown in Fig. 3. According to the diffraction cards JCPDS No. 01-080-0074 and JCPDS No 01-078-2076, the ZnO and Cu_2O have hexagonal wurtzite and cubic structures, respectively. No secondary phases are observed, neither for ZnO or for Cu_2O. In addition to the presence of ITO peak, the XRD patterns of undoped ZnO and Cu-doped ZnO show the presence of the (002) plane, demonstrating their c-axis oriented perpendicular to the substrate surface. The intensity of the (002) peak decreases for doped ZnO, which can be explained by the difference in the ionic radii between the Zn^{2+} and Cu^{2+} ions [28]. Furthermore, the peak position of the (002) plane shifts to higher angles confirming the exchange between Zn^{2+} and Cu^{2+} in the ZnO lattice [29]. The appearance of diffraction reflections for Cu_2O at 2θ= 29.56°, 36.47°, 42.40°, 61.39°, 73.57° are related to the (110), (111), (200), (220) and (311) planes, respectively. Furthermore, the high intensity of the (111) diffraction peak indicates a preferential growth of the Cu_2O thin films along the (111) direction. As for the XRD patterns of the Cu_2O/Cu-doped ZnO heterostructure, all the characteristic peaks of Cu_2O and ZnO thin films are observed. These results are consistent with the SEM observations.

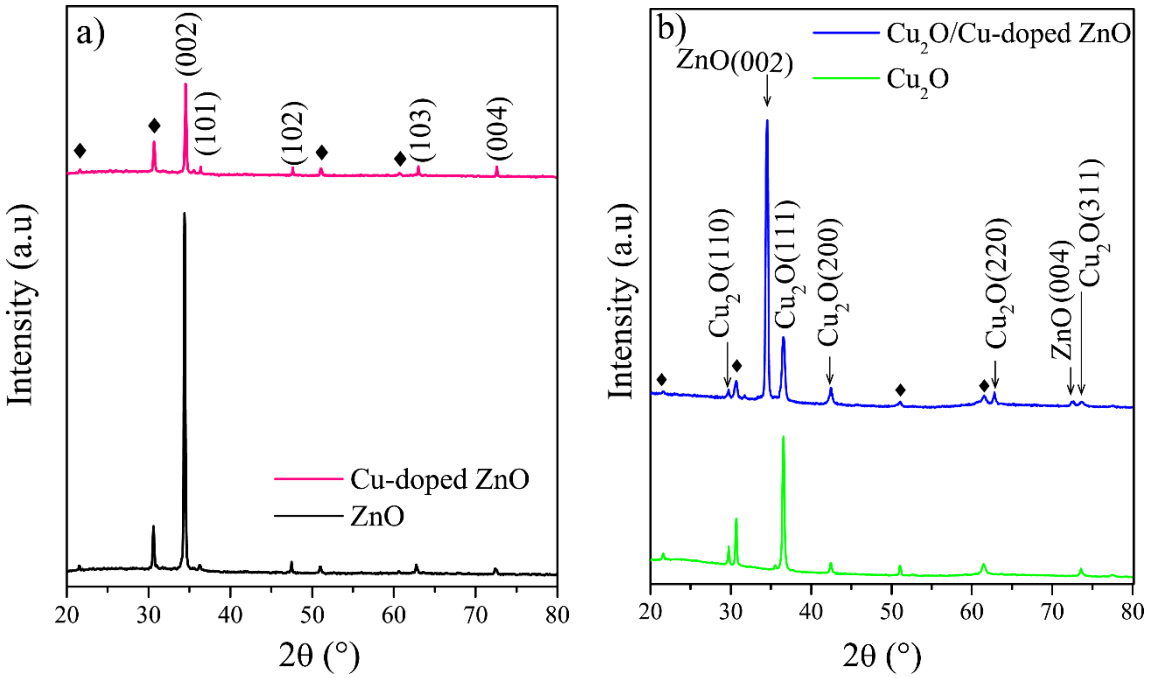

Fig. 3. XRD patterns of electrodeposited: **a)** ZnO and Cu-doped ZnO. **b)** Cu_2O and Cu_2O/Cu-doped ZnO heterojunction. The XRD peaks of the ITO substrate were marked by '♦' diamond.

The average crystallite sizes of the electrodeposited films were estimated from the full width at half maximum (FWHM) of the intensive peak using the Debye–Scherrer formula:

$$D = \frac{0.9\,\lambda}{\beta cos\theta_{(002)}} \tag{2}$$

where λ, β, and θ are the X-ray wavelength, the full width at half maximum (FWHM), and the Bragg's angle, respectively. The average crystallite size of ZnO, Cu-doped ZnO, Cu_2O, and Cu_2O/Cu-doped ZnO was 39.04 nm, 33.9 nm, 42.3 nm, and 25.67 nm, respectively.

3.3. Optical analysis

The optical characteristics of ZnO, Cu-doped ZnO, Cu_2O, and Cu_2O/Cu-doped ZnO thin films were investigated by transmission and absorption spectroscopy, with ITO glass used as a reference (Fig. 4). A high transmittance was observed for both undoped ZnO and Cu-doped ZnO, with a red shift in the absorption edge for the doped ZnO indicating the role of the doping as a window layer in the Cu_2O/Cu-doped ZnO heterojunction, allowing a large percentage of light to penetrate the absorbing layer (Cu_2O).

The exploitation of the absorbance spectra allows the estimation of the optical gap energy values using the Tauc formula [30]:

$$\alpha h\nu = B\,(h\nu - E_g)^r \quad (3)$$

where B is a constant, α is the absorption coefficient, hν is the photon energy, r is a number that depends on the electronic transition (r = ½ in our case), and E_g is the optical bandgap energy.

Fig. 4c and d show the plots of $(\alpha h\nu)^2$ vs. (hν). The optical band gap can be calculated by extrapolating the linear portion of the plot to the energy axis. The band gap energies calculated for ZnO, Cu-doped ZnO, and Cu_2O are 3.36, 3.08, and 2.17 eV respectively. However, when the p-Cu_2O and n-ZnO semiconductors come into contact, a p-n junction is created at the interface, resulting in a band alignment that promotes the electron transport from the Cu_2O conduction band to the ZnO conduction band. In this case, the estimated band gap value for Cu_2O/Cu-doped ZnO heterojunction is 2.4 eV for Cu-doped ZnO and 2.32 eV for Cu_2O. The interfacial transition between the conduction band of ZnO and the valence band of Cu_2O was estimated at 1.73 eV, which is consistent with the result of Makhlouf et al. [31]. The decrease in the band gap of Cu-doped ZnO indicates that the absorption band is shifted to higher wavelengths, while the increase in the band gap of Cu_2O indicates that the absorption band has been shifted to lower wavelengths, which is a typical behavior of heterojunction thin film material [32].

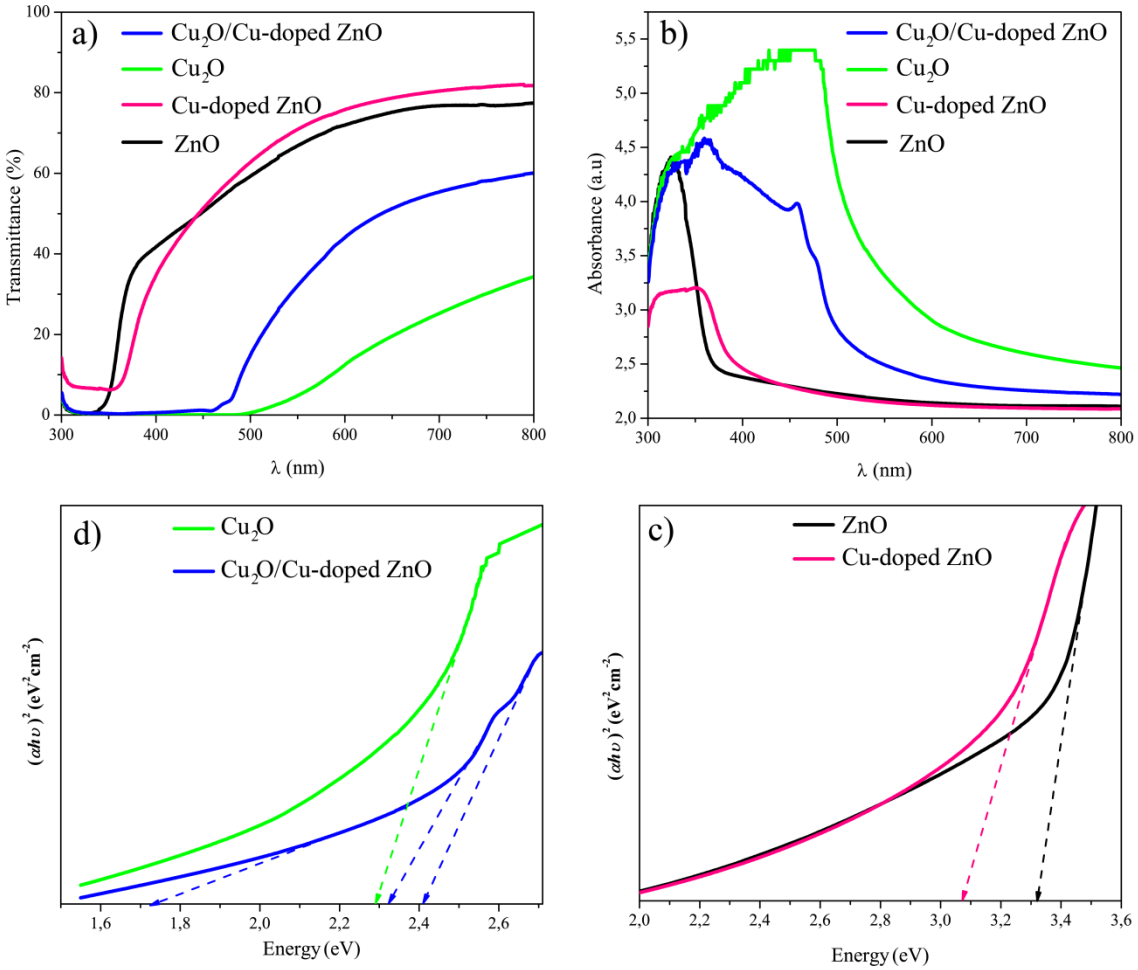

Fig. 4. a,b) transmittance and absorbance spectra of ZnO, Cu-doped ZnO, Cu_2O, and Cu_2O/Cu-doped ZnO**. c,d)** Tauc plots calculated from the UV–visible data.

3.4. XPS analysis

To further investigate the chemical state of dopant atom in Cu-doped ZnO, XPS analysis was performed. Fig. 5 shows XPS survey spectrum, the Zn-2p, and Cu-2p core level regions of the Cu-doped ZnO samples. The survey spectrum shows no organic or other contamination, consistent with EDS results. For Cu-doped ZnO spectrum, additional peaks characteristic of Cu 2p are observed which confirm again the presence of Cu in the doped sample. A doublet at 1020.7 eV and 1043.8 eV is observed in fig. 5b corresponding to the Zn-2p3/2 and 2p1/2 core levels, respectively. According to the literature, the Cu 2p1/2 and Cu 2p3/2 signals located around 952.2 and 933.6 eV, respectively revealed that Cu is in its divalent (Cu^{2+}) state [33].

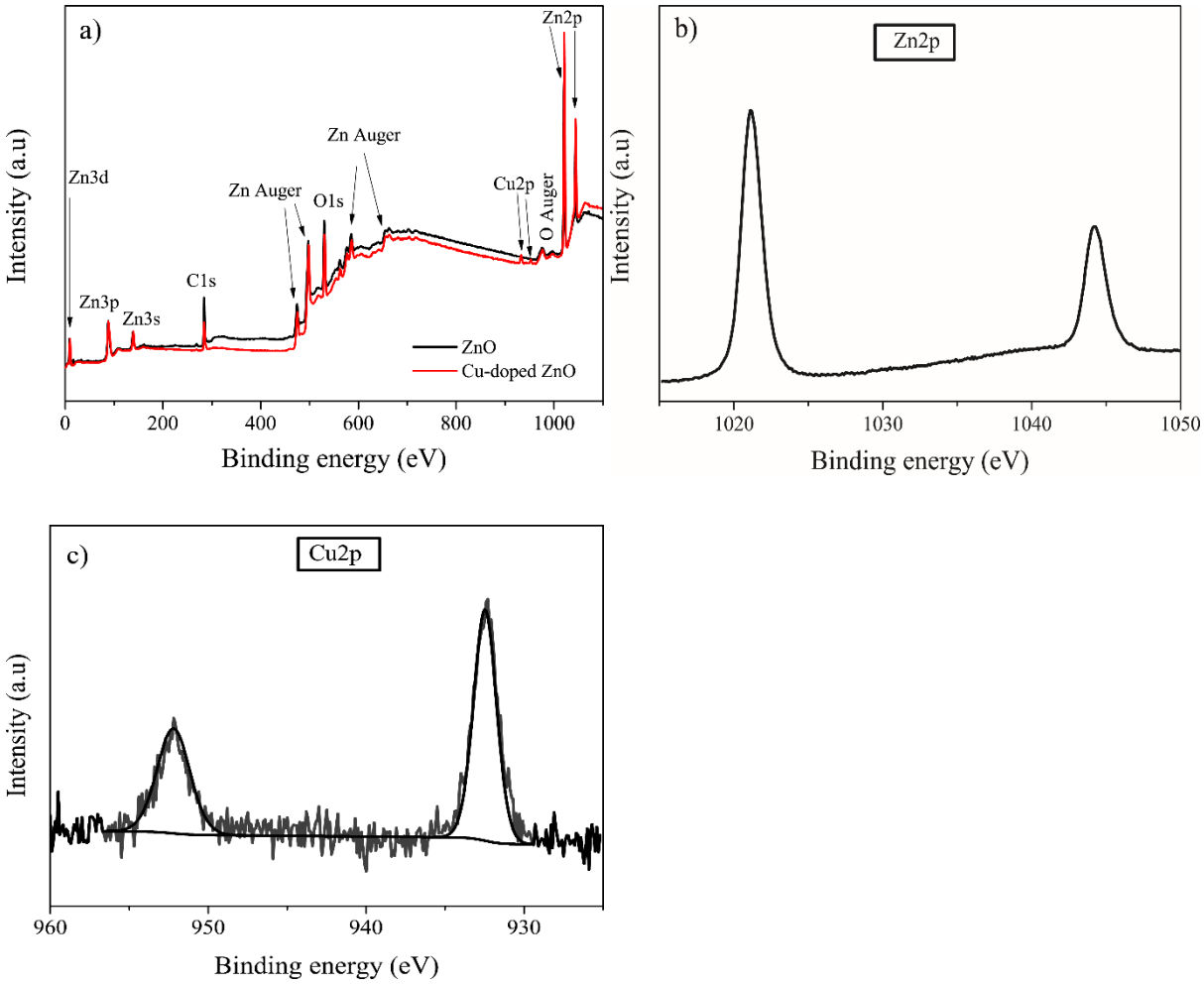

Fig. 5. XPS of a) Survey spectra b) Zn-2p, and c) Cu-2p core level of Cu-doped ZnO.

3.5. Electrochemical impedance spectroscopy measurements

To better understand the charge-transport characteristics of the electrodeposited photocatalysts, electrochemical impedance measurements were performed in 0.1 M Na_2SO_4 solution in the dark, and the results are shown as Nyquist plots in Fig. 6. As can be seen, all samples exhibit a single semicircle followed by a straight line (these points are acquired in the low-frequency region). The semicircle in the Nyquist plot is characteristic of the charge transfer process (R_{ct}) at the electrode/electrolyte interface, while the linear part indicates a process limited to mass transfer [34]. The lower the R_{ct}, the higher the charge transfer efficiency and the lower the charge recombination rate. From Fig. 6, the results show that R_{ct} = 3.678, 1.082, 0.843, 0.718, 0.452 kΩ for pure ZnO, Cu-doped ZnO, Cu_2O, Cu_2O/ZnO, and Cu_2O/Cu-doped ZnO, respectively.

The above findings clearly highlight that the combination of the n-type Cu-doped ZnO with the p-type Cu_2O heterostructure (Cu_2O/Cu-doped ZnO) significantly enhances the interfacial charge transport and the separation efficiency of photoexcited electron-hole pair [35].

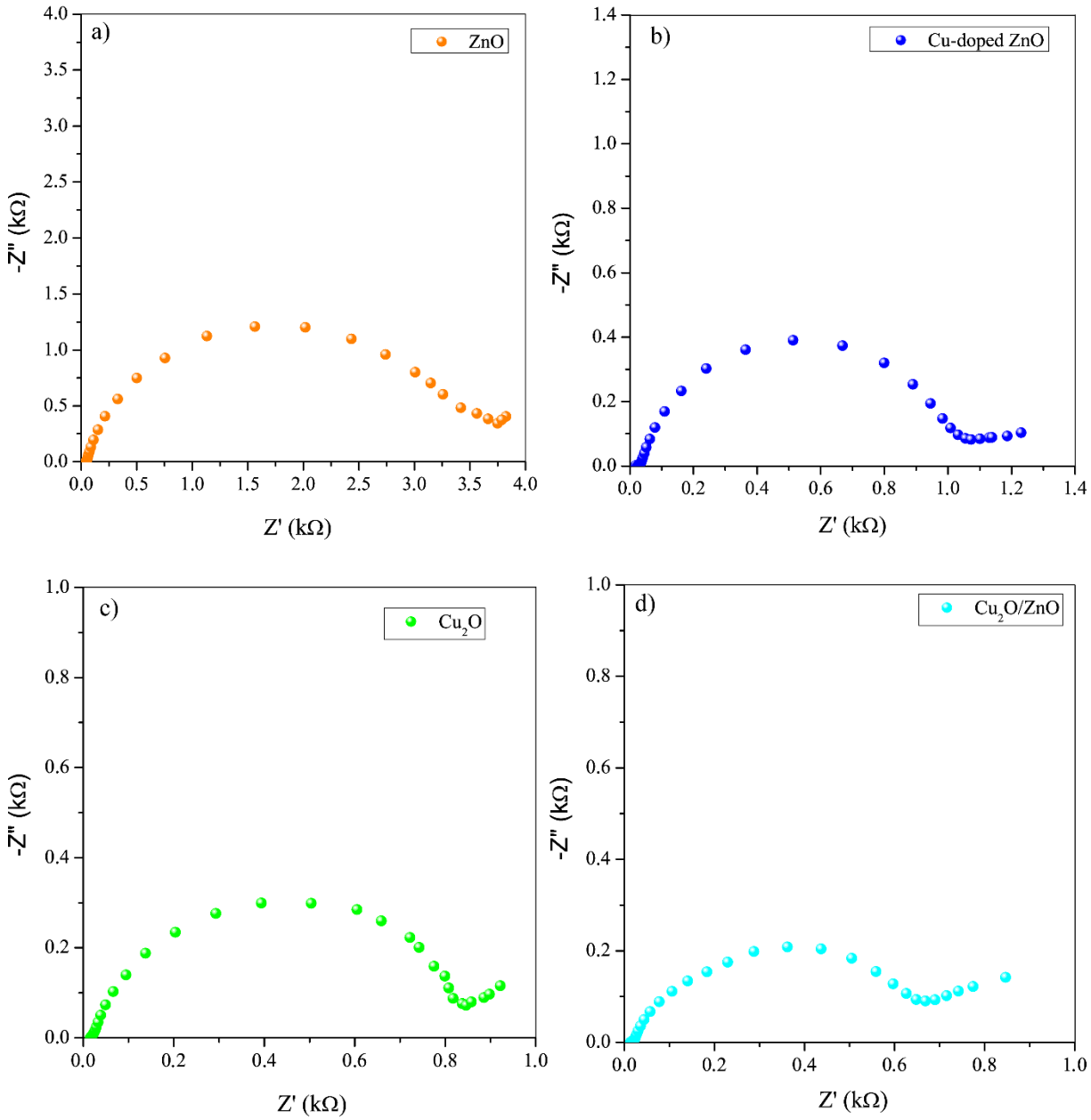

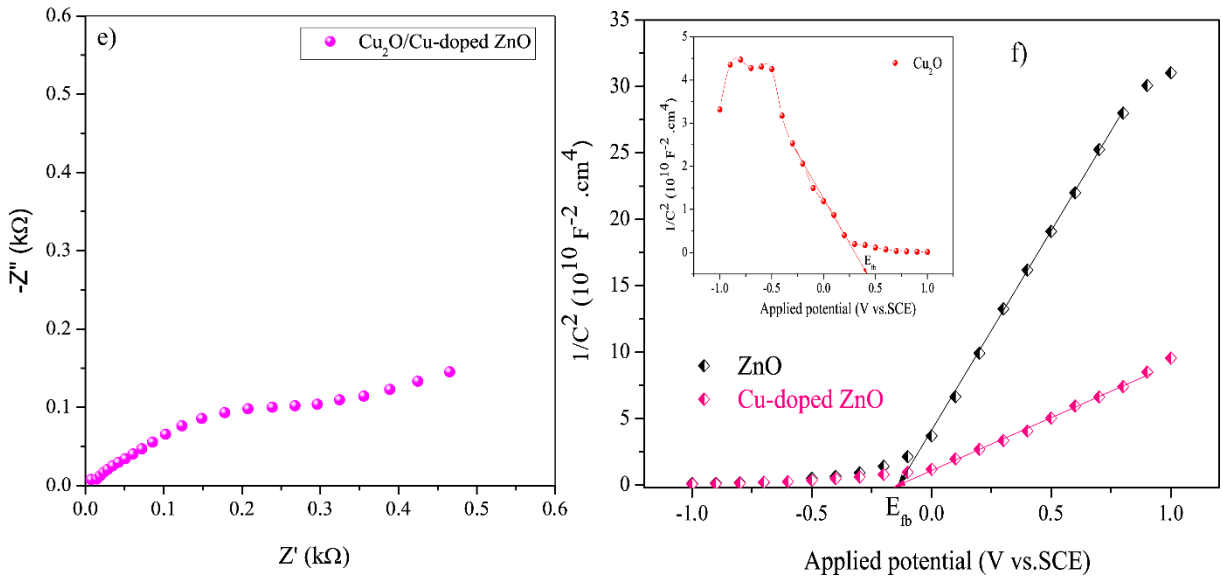

Fig. 6: Nyquist EIS plots of **a)** ZnO, **b)** Cu-doped ZnO, **c)** Cu_2O, **d)** Cu_2O/ZnO and **e)** Cu_2O/Cu-doped ZnO. **f)** Mott-Schottky plots of pure and Cu-doped ZnO, inset (Cu_2O thin film).

Mott-Schottky analysis was used to identify the type of electrical conduction and to estimate the donor concentration of ZnO, Cu-doped ZnO and Cu_2O nanostructures from capacitance-voltage measurements according to the following equation [23]:

$$\frac{1}{C_{sc}^2} = \beta\left(\frac{2}{qA^2N_D\varepsilon\varepsilon_0}\right)\left(E - E_{fb} - \frac{kT}{q}\right) \quad (4)$$

with C_{sc} the space charge capacitance, ε the dielectric constant (8.5 for ZnO) and (7.6 for Cu_2O), ε_0 the permittivity of free space (8.85×10^{-14} F/cm), A the exposed electrode area (~1 cm^2), E_{fb} the flat band potential, k the Boltzmann's constant (1.38×10^{-23} J/K), T the absolute temperature (298 K), q the electron charge (1.6021×10^{-19} C), and N_D the carrier density, β is either +1 for n-type or -1 for p-type semiconductor. As shown in Fig. 6f, for both pure and doped ZnO, the slope of the curves is positive, suggesting that the Cu dopants retain the intrinsic n-type conduction of ZnO. In contrast, the negative slope observed for the Cu_2O film (Fig. 6f, inset) indicates that this film displays p-type conduction. The carrier density ($N_{A,D}$) of the synthesized catalysts was estimated to be 4.64×10^{18} cm^{-3} for the Cu_2O thin film and 5.60×10^{19} cm^{-3} for pure ZnO. For Cu-doped ZnO, the substitution of Zn by Cu(II) ions

significantly increases the conductivity of the ZnO layer material (the carrier density is 2.05 × 10^{20} cm^{-3}). These values are within the typical range reported in the literature [30,36]. The results of Mott-Schottky analysis are in agreement with the EIS measurements.

3.6. Photocatalytic performance

3.6.1 Under UV light

Fig. 7 shows the photocatalytic activity of pure and Cu-doped ZnO in the photodegradation of the three dyes MB, CR and MO. The variation of the dye concentrations was measured by UV-visible absorption taken at characteristic absorption peaks, which are located at 660, 500 and 464 nm for MB, CR and MO respectively. Control experiments were systematically performed in the absence of photocatalyst

All dyes show a progressive decrease in the intensity of the absorption peak after 150 minutes of UV irradiation. The following differences are observed: in the presence of undoped ZnO, degradation rates of 74%, 67%, and 39% are achieved for MB, CR, and MO respectively. MO is the most difficult dye to degrade compared to MB and CR due to the high bond energy of the N═N functional group (4.33 eV) [6]. However, in the presence of Cu-doped ZnO, the photocatalytic activity shows an interesting improvement with MB, CR, and MO degradation rates of 95%, 81% and 67%, respectively. From Fig. 7 (b, e, h) it can be seen that the degradation of the dyes in the absence of photocatalyst is slow and does not exceed 10%, 12%, and 6% for MB, CR, and MO, respectively after 2.5 h of UV light exposure. Thus, the important role of the photocatalysts for the improvement of the photocatalysis process is confirmed.

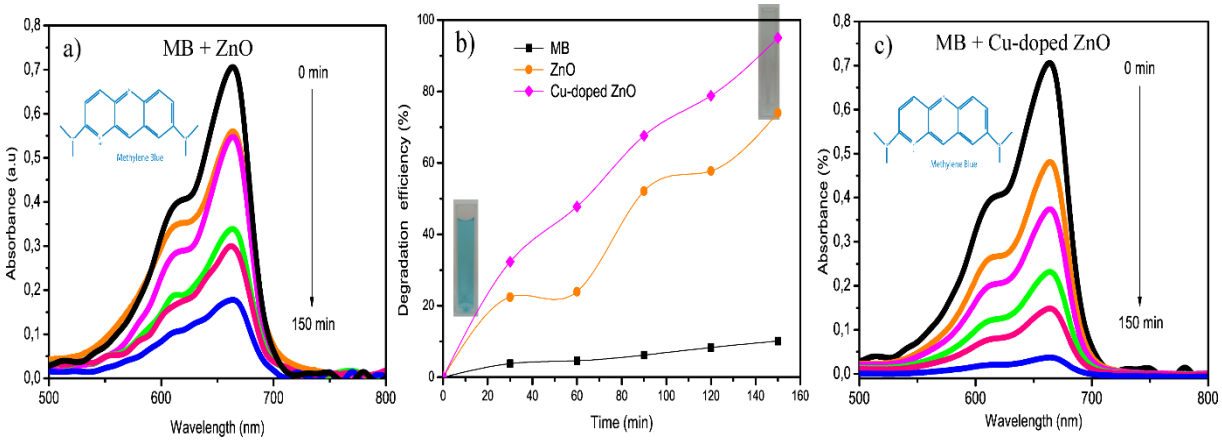

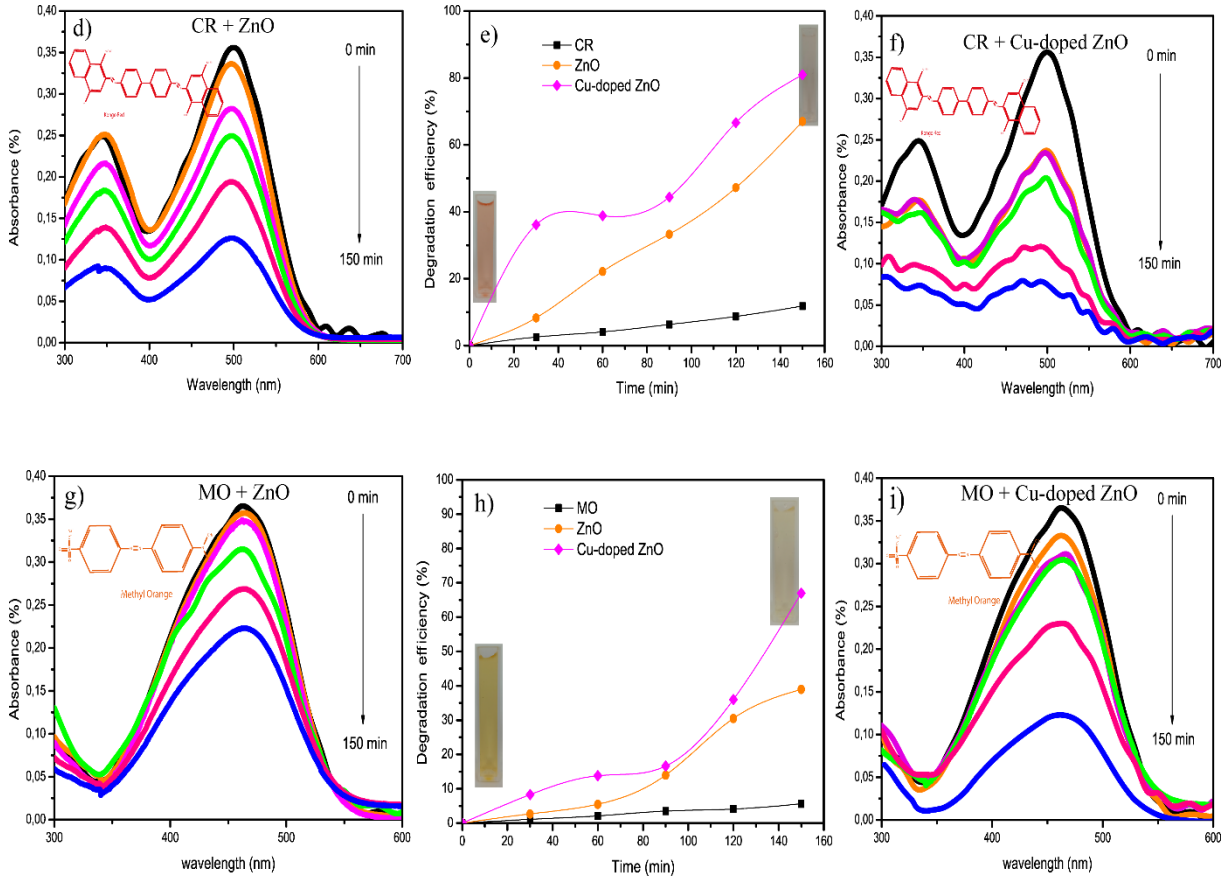

Fig. 7. UV–visible spectra and photodegradation rate curves under UV light for 150 min of MB **(a-c)**, CR **(d-f)** and MO **(g-i)**, respectively using pure and Cu-doped ZnO as catalysts.

In general, the mechanism of photocatalytic degradation under UV irradiation consists of the following three main steps: the first step is the excitation of the semiconductor charge carriers, inducing the migration of electrons into the conduction band and an equal number of holes in the valence band. Next, the electron-hole pairs formed generate hydroxyl (•OH) and superoxide radicals ($\bullet O_2^-$) with high oxidation properties. Finally, these radicals react with the organic substances and trigger the reaction sequence to form the final products. The main drawback of ZnO as a photocatalyst is the rapid recombination of the photo-excited electron-hole pairs [37,38]. Doping ZnO nanorods with Cu enables the exchange of some Zn atoms by Cu atoms, thus creating new energy levels in the band gap of ZnO. The photoexcited electrons are accepted by the new energy level(s) of Cu^{2+} which is reduced to Cu^{+}. This reduction process extends the lifetime of the electron-hole pairs of the semiconductor, allowing more photons to be harvested during the photodegradation process (Fig. 8). As a result, the

production of hydroxyl radicals is accelerated which thus increases the photocatalytic activity of Cu-doped ZnO catalyst for dye degradation compared to undoped ZnO [18].

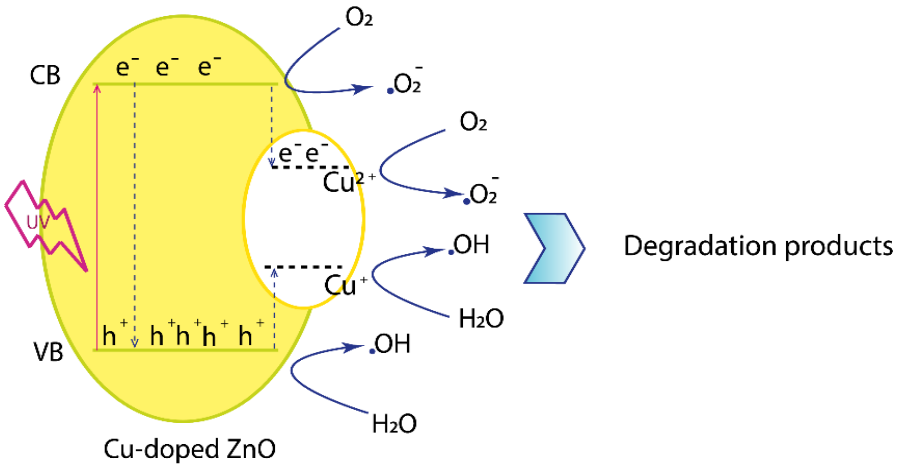

Fig. 8. Schematic band diagram of Cu-doped ZnO showing the charge separation and transportation processes for the photocatalytic degradation of the dyes Methylene blue, Methyl orange and Congo red.

The photodegradation reaction kinetics of dyes was evaluated using the first order model given by the following equation [39]:

$$ln\frac{C}{C_t} = kt \quad (5)$$

where C is the initial concentration and C_t is the concentration of the dye at the reaction time t, k is the rate constant. From Fig. 9, the linear relationship, observed between the irradiation time and $\ln(C/C_t)$ values with a correlation coefficient $R^2 > 0.9562$, confirms that the photocatalytic degradation kinetics follows the first order reaction [40].

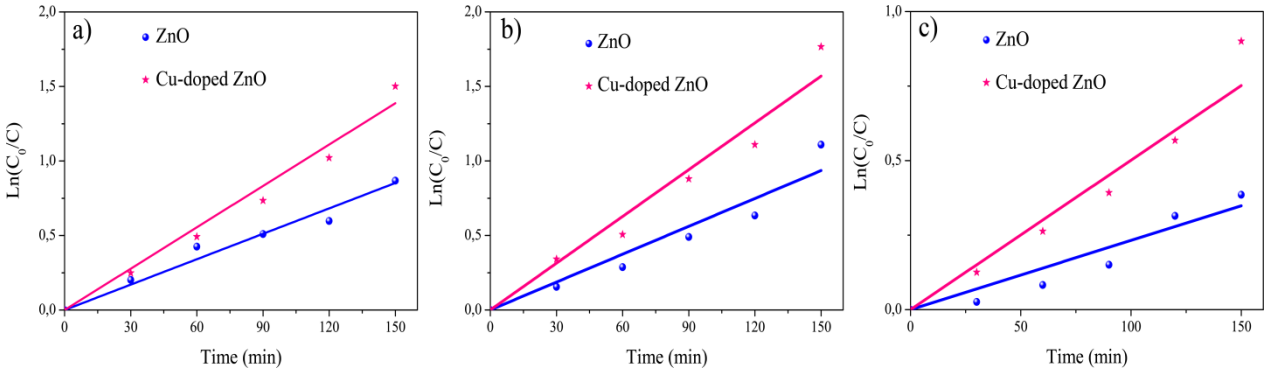

Fig. 9. Photo-catalytic kinetic curves under UV light of: **a)** MB, **b)** CR and **c)** MO obtained with pure and Cu-doped ZnO as catalysts.

The degradation rate constants (k) of the three dyes were determined from the data fitted by equation (5) and the values are given in Table 1. As expected, the Cu-doped ZnO photocatalyst shows highest rate constant compared to pure ZnO and almost completely degrades the MB dye within 150 min. These results reveal that Cu doping accelerates the degradation process and enhances its efficiency.

Table 1 Reaction rate constants (k), degradation efficiency (D) and R^2 values of the kinetic data fit by first order model for the dyes MB, MO and CR with the ZnO and Cu-doped ZnO catalysts under UV light.

	Methylene blue			**Congo red**			**Methylene orange**		
	k (min^{-1})	**R^2**	**D (%)**	**K (min^{-1})**	**R^2**	**D (%)**	**k (min^{-1})**	**R^2**	**D (%)**
ZnO	0.0056	0.9623	74	0.006	0.9594	67	0.0023	0.9582	39
Cu-doped ZnO	0.0091	0.9642	95	0.01	0.9597	81	0.005	0.9668	67

3.6.2 Under natural sunlight

ZnO is a material that absorbs photons with an energy close to the ultraviolet (less than 400 nm) and, due to its high bandgap energy, ZnO as a catalyst is only able to utilize a very small fraction of the solar spectrum, absorbing less than 5 % of sunlight incident on its surface.

Coupling ZnO with a material that can be excited in the visible region is considered a promising solution [37].

In this section, Cu-doped ZnO, Cu_2O and Cu_2O/Cu-doped ZnO were used as photocatalysts in the photocatalytic degradation under solar irradiation of the three dyes with the same conditions as used in the photocatalytic degradation experiments under UV light. Fig. 10 shows the photodegradation of the three dyes MB, CR and MO in the absence and presence of the Cu-doped ZnO, Cu_2O and Cu_2O/Cu-doped ZnO thin film photocatalysts. As observed, the degradation efficiency for all dyes is negligible under solar irradiation in the absence of photocatalysts (Fig. 10a, d, g). On the other hand, in the presence of the photocatalysts, the absorption peaks of the three dyes in the aqueous solution gradually decrease over time (Fig. 10c, f, i). Using Cu-doped ZnO or Cu_2O separately as photocatalyst, a decrease in the absorption maxima for all three dyes (Fig. 10b, e, h) is observed after 120 min. The highest degradation efficiency is observed for the Cu_2O/Cu-doped ZnO material combination with 86%, 78% and 96% for MB, MO and CR, respectively. The improvement of the performance can be attributed to the combination of two factors: on the one hand, the use of doped zinc oxide (Cu-doped ZnO) improves the efficiency in the ultraviolet region of the sunlight, while the addition of Cu_2O prolonged the absorption in the visible light region. On the other hand, the combination of doping and coupling strategies increases the charge separation and the lifetime of the electron-hole pairs. The degradation efficiencies are summarized in Table 2.

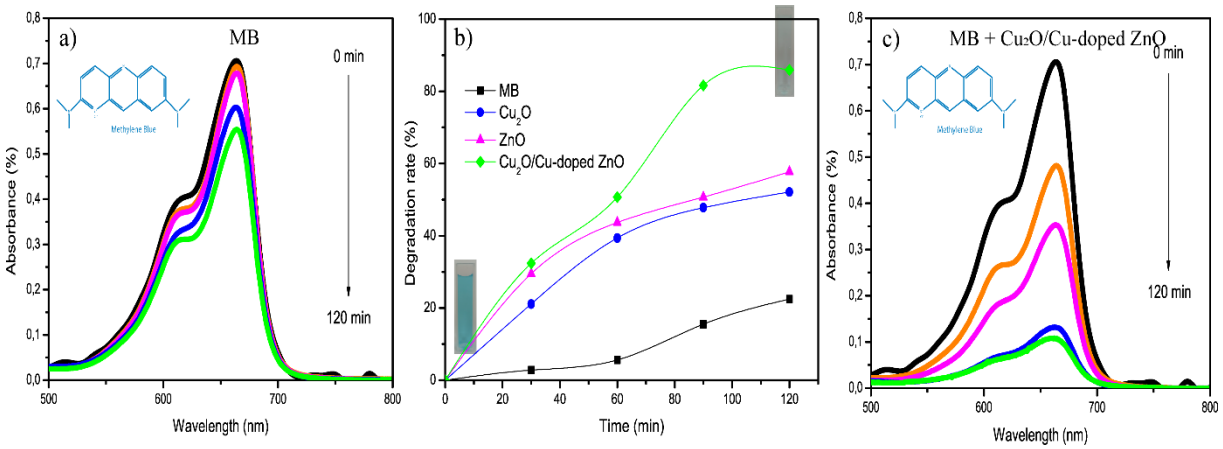

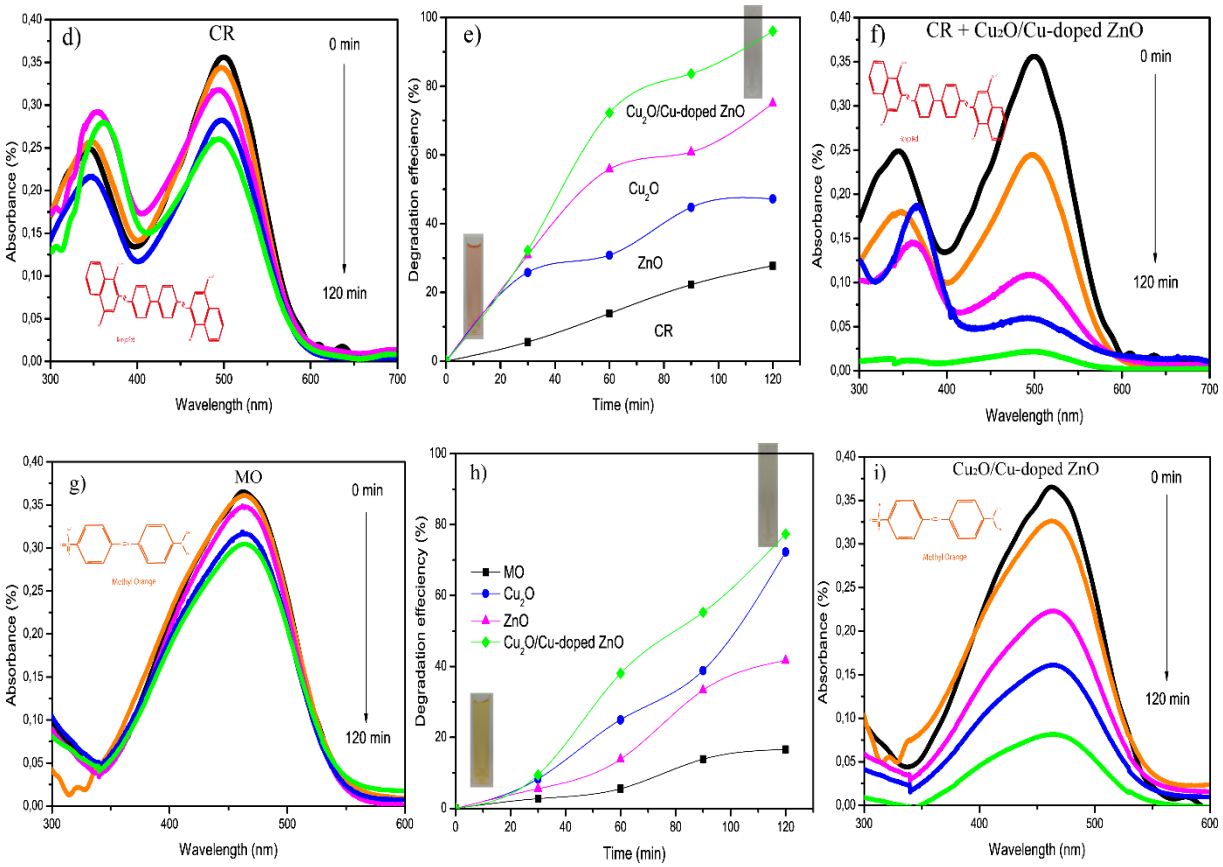

Fig. 10. UV–visible spectra and photodegradation rate curves under sunlight of: **(a-c)** MB, **(d-f)** CR and **(g-i)** MO using Cu-doped ZnO, Cu_2O and Cu_2O/Cu-doped ZnO as catalysts.

When the semiconductors n-ZnO and p-Cu_2O are combined, a heterojunction is created which induces a concentration gradient of charge carriers at the interface. To achieve equilibrium, electrons move from ZnO to Cu_2O, while holes move in the opposite direction. Thus, an internal electric field is created at the junction, which could alter the charge carrier transfer during the photocatalytic reaction. When visible light is used to irradiate such a photocatalyst, the previous equilibrium state is disturbed and the photoexcited pairs (e^-, h^+) can be excited in Cu_2O and separated at the interface of Cu_2O/ZnO. As the E_C of Cu_2O is higher than that of ZnO, the photogenerated electrons from Cu_2O CB are transferred in ZnO CB and can react with the oxygen species adsorbed on the photocatalyst surface producing $\bullet O_2^-$. The returned electrons are trapped by the Cu levels which further enhances the separation of the photoexcited electron-hole pairs [18]. Besides, the h^+ remaining in the valence band of Cu_2O can react with OH^- to form •OH. These radicals are highly reactive due to their strong oxidizing properties and can lead to partial or complete degradation of organic compounds by forming harmless products such as CO_2, H_2O and N_2 (Fig. 11). The increased amounts of

•O_2^- and •OH boost the photocatalytic performance, while the heterogeneous p-n structure favors the separation of electrons and holes, and effectively suppresses their recombination by the internal electric field [41–43].

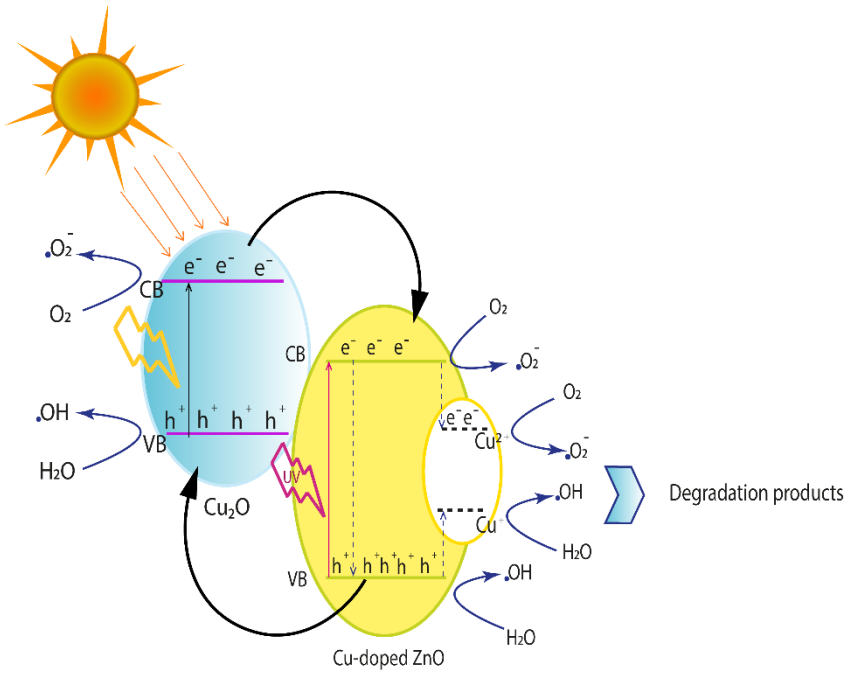

Fig. 11. Schematic band diagram of Cu_2O/Cu-doped ZnO nanostructures showing the charge separation and transportation processes for photocatalytic degradation of dyes.

Fig. 12 depicts the plots of $\ln(C/C_t)$ versus the irradiation time. The reaction rate constant (k) was extracted from the slope of the linear fitted line and the values are listed in Table 2.

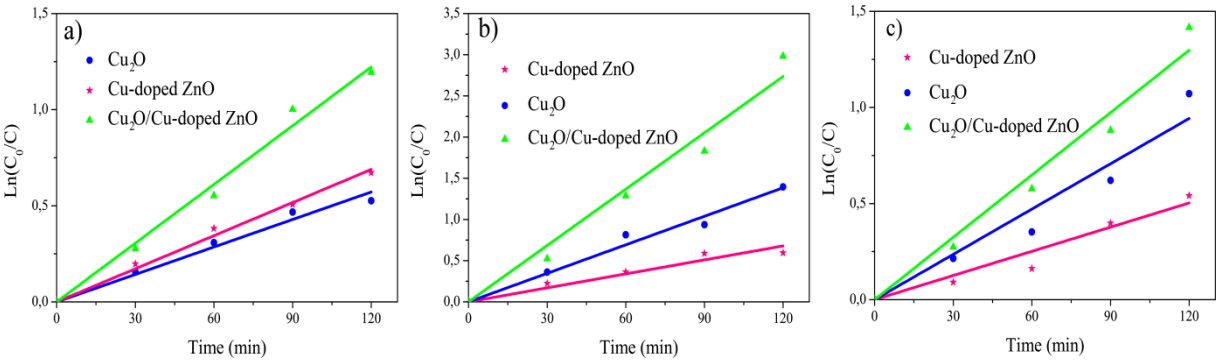

Fig. 12. The kinetic curves of photo-catalytical degradation under sunlight of: **a)** MB, **b)** CR and **c)** MO obtained with Cu_2O, Cu-doped ZnO and Cu_2O/Cu-doped ZnO as photocatalysts.

The observed linear relationship between the irradiation time and $\ln(C/C_t)$ values and the correlation coefficient $R^2 > 0.9562$ indicate that the photocatalytic degradation kinetics under sunlight follows the first order reaction [40]. As expected, the Cu_2O/Cu-doped ZnO heterojunction exhibits a higher rate constant than that of Cu_2O and Cu-doped ZnO, confirming the benefit of the doping and coupling strategies to increase the photocatalytic activity.

Table 2 Reaction rate constants, degradation efficiency (D), and R^2 values of the kinetic data fit by first order model for MB, MO and CR on Cu-doped ZnO, Cu_2O and Cu_2O/Cu-doped ZnO under solar light.

	Methylene blue			**Congo red**			**Methyl orange**		
	K (min^{-1})	**R^2**	**D (%)**	**k (min^{-1})**	**R^2**	**D (%)**	**k (min^{-1})**	**R^2**	**D (%)**
Cu-doped ZnO	0.0057	0.9965	58	0.0056	0.9760	47	0.0042	0.9711	42
Cu_2O	0.0047	0.9912	52	0.0154	0.9910	75	0.0078	0.9718	72
Cu_2O/Cu-doped ZnO	0.0108	0.9945	86	0.0227	0.9874	96	0.0101	0.9881	78

3.7. Scavenger test

The trapping experiments of the main reactive species were carried out using different scavengers such as EDTA-2Na, L-ascorbic acid, and isopropyl alcohol (IPA) to trap holes (h^+), $\bullet O_2^-$, and •OH, respectively. Fig. 13 shows the photodegradation efficiency of MB, MO, and CR solutions containing different scavengers over Cu-doped ZnO under UV light and Cu_2O/Cu-doped ZnO under sun light. It is clearly from fig. 13a, the photocatalytic degradation efficiency of Cu-doped ZnO shows an important decrease by the addition of IPA and L-ascorbic acid, indicating that •OH and $\bullet O_2^-$ are the main active species for the degradation of the three dyes. Besides, the photocatalytic degradation with the addition of ascorbic acid is lower than that of the addition of IPA, revealing that $\bullet O_2^-$ radicals are more important oxidative species for the degradation of MB under UV light. In the other hand, the same observation for Cu_2O/Cu-doped ZnO as photocatalyst under the sun light, where •OH and $\bullet O_2^-$ radicals are the main active species for the degradation of the three dyes. Moreover,

the addition of IPA showed significant reduction in CR degradation indicating that •OH species are actively involved in the degradation process.

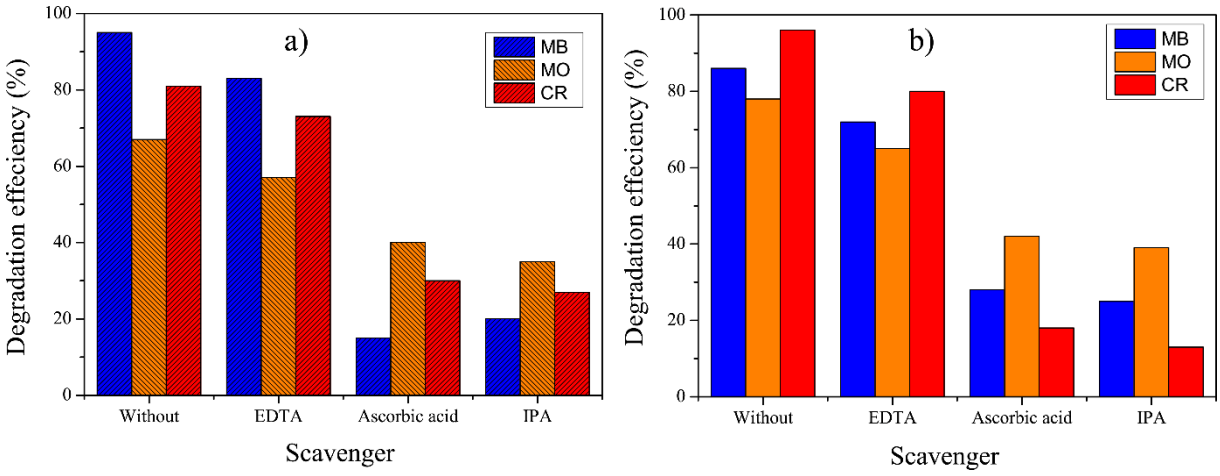

Fig. 13. Degradation efficiency in the presence of different scavengers over: **a)** Cu-doped ZnO under UV-light. **b)** Cu_2O/Cu-doped ZnO under sun light.

3.8. Reusability experiment

To test the photocatalytic stability of the photocatalysts Cu-doped ZnO and Cu_2O/Cu-doped ZnO films were used for the recyclability experiment. The choice of the Cu_2O/Cu-doped ZnO thin film as catalyst is based on the use of natural source light (sun irradiation) where the heterojunction exhibited better performance for the degradation of Congo red where Cu-doped ZnO exhibited better performance for the degradation of Methylene blue under UV light. The thin-films catalysts were washed for reuse again after each cycle. Fig. 14 shows the performance of the catalysts in a series of experiments. From fig.14a, the degradation efficiency remained at about 90% in the fourth reusability experiment for Cu_2O/Cu-doped ZnO films. This shows that more than 90% of degradation efficiency was still present even after the fourth cycle. Where Cu-doped ZnO retained a good degradation capacity after three cycles (fig.14b). The results suggest an acceptable stability and repeatability of the Cu_2O/Cu-doped ZnO hetero-system and Cu-doped ZnO for the photocatalytic degradation of Congo red and Methylene blue, respectively.

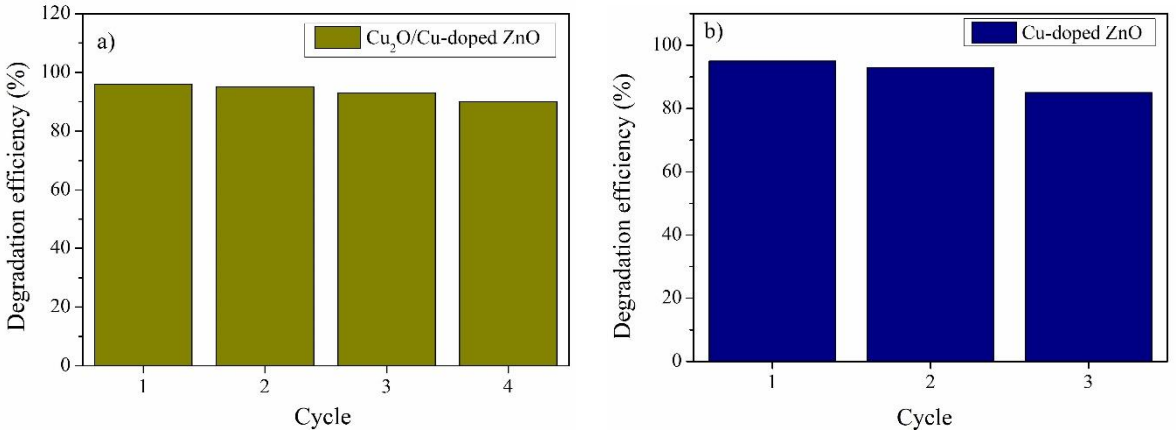

Fig. 14. reusability experiment over successive cycles in the presence of: a) Cu_2O/Cu-doped ZnO under sunlight, b) Cu-doped ZnO under UV light.

At this point, it is interesting to compare the photocatalytic performance obtained with our photocatalysts with those reported in the literature. Table 3 shows the photocatalytic efficiency of selected photocatalysts published in the literature for various organic pollutants. One can see that the nanostructured photocatalytic heterosystem developed in this study shows remarkable photocatalytic activity compared to other catalysts described in the literature. Such promising improvement is mainly due to the synergistic effect of Cu_2O material (bandgap of 2.2 eV) which absorbs in the visible region and of Cu-doped ZnO material (bandgap of 3.08 eV) which is absorbs UV part from the solar light.

Table 3. Degradation efficiency of MB, CR and MO with other photocatalysts thin film reported in the literature.

Material	Dye	Degradation rate (%)	Time	Light source	Ref.
ZnO@CuO	CR	90	300 min	Visible light	[44]
Cu-doped ZnO	CR	81	150 min	UV light	This work
Cu_2O/Cu-doped ZnO	CR	96	120 min	Sun radiation	This work
ZnO	MB	86	180 min	UV light	[6]
Au–Pd /Cu_2O/ZnO	MB	77	120 min	UV light	[42]
ZnO	MB	90	240 min	UV light	[45]

Cu-doped ZnO	MB	95	150 min	UV light	This work
Ag/ZnO	MB	100	90 min	Visible light	[46]
Co doped ZnO	MB	63	140 min	Visible light	[47]
Cu-doped ZnO	MB	43	140 min	Visible light	[47]
Cu_2O/Cu-doped ZnO	MB	86	120 min	Sun radiation	This work
ZnO	MO	49	180 min	UV light	[6]
Cu-doped ZnO	MO	67	150 min	UV light	This work
ZnO	MO	80	240 min	Visible light	[48]
ZnO	MO	53	360 min	Sun radiation	[5]
Cu_2O	MO	82	360 min	Sun radiation	[5]
Cu_2O/Cu-doped ZnO	MO	78	120 min	Sun radiation	This work

4. Conclusion

In summary, in order to avoid the effort and cost of recovering photocatalytic nanoparticles from suspensions after water treatment, pure ZnO, Cu-doped ZnO and Cu_2O thin solid film were used as photocatalysts. Their photocatalytic activity was tested for the photocatalytic degradation of the three common organic dyes. The photocatalysts were irradiated with UV and natural sunlight.

The results showed that Cu-doped ZnO performed better performance under UV light than undoped ZnO, owing to the fact that doping extended the lifetime of the photoexcited electron-hole pairs of the semiconductor, allowing more photons to be harvested during the photodegradation process. Among the dyes used, the degradation of Methylene blue is almost complete after 150 min, with 95% of the dye molecules removed, revealing that Cu doping not only enhances the degradation efficiency, but also makes it faster compared to undoped degradation. In the second part, we replaced the UV light source with sun radiation (a free natural source). In this case, Cu_2O was used as an absorber layer in the visible region.

The results showed that the combination between the Cu-doped ZnO and Cu_2O materials improved the photocatalytic process with the example of the Congo red being completely degraded in 120 min. The improvement was made at the optical level with the use of doped zinc oxide (Cu-doped ZnO) which enhanced the activation of ZnO in the ultraviolet range of sunlight, and the combination of Cu-doped ZnO with Cu_2O which extended the absorption in the visible region. Moreover, at the energetic level, the combining of doping and coupling strategies increased the charge separation and lifetime of the electron-hole pairs.

This study provides future directions for the synthesis and application of p-n heterojunction thin films for the removal of organic dyes, by extending the absorption in the visible light, and by increasing the charge separation and the lifespan of the electron-hole pairs.

References

[1] J. Theerthagiri, S. Salla, R.A. Senthil, P. Nithyadharseni, A. Madankumar, P. Arunachalam, T. Maiyalagan, H.S. Kim, A review on ZnO nanostructured materials: Energy, environmental and biological applications, Nanotechnology. 30 (2019). https://doi.org/10.1088/1361-6528/ab268a.

[2] D.K. Sharma, S. Shukla, K.K. Sharma, V. Kumar, A review on ZnO: Fundamental properties and applications, Mater. Today Proc. (2020). https://doi.org/10.1016/j.matpr.2020.10.238.

[3] S. Shahzad, S. Javed, M. Usman, A Review on Synthesis and Optoelectronic Applications of Nanostructured ZnO, Front. Mater. 8 (2021) 1–16. https://doi.org/10.3389/fmats.2021.613825.

[4] I.S. Brandt, M.A. Tumelero, S. Pelegrini, G. Zangari, A.A. Pasa, Electrodeposition of Cu2O: growth, properties, and applications, J. Solid State Electrochem. 21 (2017) 1999–2020. https://doi.org/10.1007/s10008-017-3660-x.

[5] A. Boughelout, R. Macaluso, M. Kechouane, M. Trari, Photocatalysis of rhodamine B and methyl orange degradation under solar light on ZnO and Cu2O thin films, React. Kinet. Mech. Catal. 129 (2020) 1115–1130.

[6] Y.G. Habba, M. Capochichi- Gnambodoe, L. Serairi, Y. Leprince- Wang, Enhanced photocatalytic activity of ZnO nanostructure for water purification, Phys. Status Solidi. 253 (2016) 1480–1484.

[7] B.A. Koiki, O.A. Arotiba, Cu2O as an emerging semiconductor in photocatalytic and photoelectrocatalytic treatment of water contaminated with organic substances: A review, RSC Adv. 10 (2020) 36514–36525. https://doi.org/10.1039/d0ra06858f.

[8] S. Boudiaf, N. Nasrallah, M. Mellal, B. Belhamdi, C. Belabed, M.A. Djilali, M. Trari, Kinetic studies of Congo Red Photodegradation on the hetero-system CoAl2O4/ZnO with a stirred reactor under solar light, J. Environ. Chem. Eng. 9 (2021) 105572. https://doi.org/10.1016/j.jece.2021.105572.

[9] A.M. Taddesse, M. Alemu, T. Kebede, Enhanced photocatalytic activity of pnn heterojunctions ternary composite Cu2O/ZnO/Ag3PO4 under visible light irradiation, J. Environ. Chem. Eng. 8 (2020) 104356.

[10] F. Moulai, O. Fellahi, B. Messaoudi, T. Hadjersi, L. Zerroual, Electrodeposition of nanostructured γ-MnO2 film for photodegradation of Rhodamine B, Ionics (Kiel). 24 (2018) 2099–2109. https://doi.org/10.1007/s11581-018-2440-7.

[11] J. Ambigadevi, P. Senthil Kumar, D.V.N. Vo, S. Hari Haran, T.N. Srinivasa Raghavan,

Recent developments in photocatalytic remediation of textile effluent using semiconductor based nanostructured catalyst: A review, J. Environ. Chem. Eng. 9 (2021) 104881. https://doi.org/10.1016/j.jece.2020.104881.

[12] S. Natarajan, H.C. Bajaj, R.J. Tayade, Recent advances based on the synergetic effect of adsorption for removal of dyes from waste water using photocatalytic process, J. Environ. Sci. 65 (2018) 201–222.

[13] I.M.F. Cardoso, R.M.F. Cardoso, J.C.G. Esteves da Silva, Advanced oxidation processes coupled with nanomaterials for water treatment, Nanomaterials. 11 (2021). https://doi.org/10.3390/nano11082045.

[14] E.M. Cuerda-Correa, M.F. Alexandre-Franco, C. Fernández-González, Advanced oxidation processes for the removal of antibiotics from water. An overview, Water (Switzerland). 12 (2020). https://doi.org/10.3390/w12010102.

[15] M. Brienza, I.A. Katsoyiannis, Sulfate radical technologies as tertiary treatment for the removal of emerging contaminants from wastewater, Sustain. 9 (2017) 1–18. https://doi.org/10.3390/su9091604.

[16] W.S. Koe, J.W. Lee, W.C. Chong, Y.L. Pang, L.C. Sim, An overview of photocatalytic degradation: photocatalysts, mechanisms, and development of photocatalytic membrane, Environ. Sci. Pollut. Res. 27 (2020) 2522–2565.

[17] M.A. Johar, R.A. Afzal, A.A. Alazba, U. Manzoor, Photocatalysis and Bandgap Engineering Using ZnO Nanocomposites, Adv. Mater. Sci. Eng. 2015 (2015). https://doi.org/10.1155/2015/934587.

[18] Q. Ma, X. Yang, X. Lv, H. Jia, Y. Wang, Cu doped ZnO hierarchical nanostructures: morphological evolution and photocatalytic property, J. Mater. Sci. Mater. Electron. 30 (2019) 2309–2315.

[19] A. Henni, A. Merrouche, L. Telli, A. Karar, F.I. Ezema, H. Haffar, Optical, structural, and photoelectrochemical properties of nanostructured ln-doped ZnO via electrodepositing method, J. Solid State Electrochem. 20 (2016) 2135–2142.

[20] D. Selloum, A. Henni, A. Karar, A. Tabchouche, N. Harfouche, O. Bacha, S. Tingry, F. Rosei, Effects of Fe concentration on properties of ZnO nanostructures and their application to photocurrent generation, Solid State Sci. 92 (2019) 76–80.

[21] J. Ge, Y. Zhang, Y.-J. Heo, S.-J. Park, Advanced design and synthesis of composite photocatalysts for the remediation of wastewater: A review, Catalysts. 9 (2019) 122.

[22] M.H. Tran, J.Y. Cho, S. Sinha, M.G. Gang, J. Heo, Cu2O/ZnO heterojunction thin-film solar cells: the effect of electrodeposition condition and thickness of Cu2O, Thin Solid

Films. 661 (2018) 132–136.

[23] T. Özdal, H. Kavak, Fabrication and characterization of ZnO/Cu2O heterostructures for solar cells applications, Superlattices Microstruct. 146 (2020).

[24] R. Kara, H. Lahmar, L. Mentar, R. Siab, F. Kadirgan, A. Azizi, Electrochemical growth and characterization of Cu2O: Na/ZnO heterojunctions for solar cells applications, J. Alloys Compd. 817 (2020) 152748.

[25] Y. Keriti, R. Brahimi, Y. Gabes, S. Kaci, M. Trari, Physical and photo-electrochemical properties of CuO thin film grown on µc-Si: H/glass. Application to solar energy conversion, Sol. Energy. 206 (2020) 787–792.

[26] F.Z. Nouasria, D. Selloum, A. Henni, D. Zerrouki, S. Tingry, Gradient doping of Cu(I) and Cu(II) in ZnO nanorod photoanode by electrochemical deposition for enhanced photocurrent generation, Ceram. Int. 47 (2021) 19743–19751. https://doi.org/10.1016/j.ceramint.2021.03.312.

[27] M.A. Hossain, R. Al-Gaashani, H. Hamoudi, M.J. Al Marri, I.A. Hussein, A. Belaidi, B.A. Merzougui, F.H. Alharbi, N. Tabet, Controlled growth of Cu2O thin films by electrodeposition approach, Mater. Sci. Semicond. Process. 63 (2017) 203–211.

[28] F. Ghahramanifard, A. Rouhollahi, O. Fazlolahzadeh, Electrodeposition of Cu-doped p-type ZnO nanorods ; effect of Cu doping on structural , optical and photoelectrocatalytic property of ZnO nanostructure, Superlattices Microstruct. 114 (2018) 1–14.

[29] P. Jongnavakit, P. Amornpitoksuk, S. Suwanboon, N. Ndiege, Preparation and photocatalytic activity of Cu-doped ZnO thin films prepared by the sol-gel method, Appl. Surf. Sci. 258 (2012) 8192–8198.

[30] M. Yarahmadi, H. Maleki-Ghaleh, M.E. Mehr, Z. Dargahi, F. Rasouli, M.H. Siadati, Synthesis and characterization of Sr-doped ZnO nanoparticles for photocatalytic applications, J. Alloys Compd. 853 (2021) 157000.

[31] H. Makhlouf, O. Messaoudi, A. Souissi, I. Ben Assaker, M. Oueslati, M. Bechelany, R. Chtourou, Tuning of Ag doped core-shell ZnO NWs/Cu2O grown by electrochemical deposition, Mater. Res. Express. 2 (2015) 95002. https://doi.org/10.1088/2053-1591/2/9/095002.

[32] E. Archela, L.P. de Camargo, M.R. da S. Pelissari, L.H. Dall'Antonia, n-ZnO/p-Cu 2 O heterojunction electrode: Characterization and evaluation of their photoelectrochemical properties, Int. J. Electrochem. Sci. 14 (2019) 3581–3594. https://doi.org/10.20964/2019.04.04.

[33] L. Chow, O. Lupan, G. Chai, H. Khallaf, L.K. Ono, B.R. Cuenya, I.M. Tiginyanu, V. V Ursaki, V. Sontea, A. Schulte, Synthesis and characterization of Cu-doped ZnO one-dimensional structures for miniaturized sensor applications with faster response, Sensors Actuators A Phys. 189 (2013) 399–408.

[34] I.Y. Bouderbala, A. Herbadji, L. Mentar, A. Azizi, Optical, structural, and photoelectrochemical properties of nanostructured Cl-doped Cu2O via electrochemical deposition, Solid State Sci. 83 (2018) 161–170. https://doi.org/10.1016/j.solidstatesciences.2018.07.015.

[35] H. Lahmar, F. Setifi, A. Azizi, G. Schmerber, A. Dinia, On the electrochemical synthesis and characterization of p-Cu2O/n-ZnO heterojunction, J. Alloys Compd. 718 (2017) 36–45. https://doi.org/10.1016/j.jallcom.2017.05.054.

[36] F. Rasouli, A. Rouhollahi, F. Ghahramanifard, Gradient doping of copper in ZnO nanorod photoanode by electrodeposition for enhanced charge separation in photoelectrochemical water splitting, Superlattices Microstruct. 125 (2019) 177–189.

[37] J. Ambigadevi, P.S. Kumar, D.-V.N. Vo, S.H. Haran, T.N.S. Raghavan, Recent developments in photocatalytic remediation of textile effluent using semiconductor based nanostructured catalyst: a review, J. Environ. Chem. Eng. (2020) 104881.

[38] A. Henni, N. Harfouche, A. Karar, D. Zerrouki, F.X. Perrin, F. Rosei, Synthesis of graphene–ZnO nanocomposites by a one-step electrochemical deposition for efficient photocatalytic degradation of organic pollutant, Solid State Sci. 98 (2019) 106039.

[39] M. Asgharian, M. Mehdipourghazi, B. Khoshandam, N. Keramati, Photocatalytic degradation of methylene blue with synthesized rGO / ZnO / Cu, Chem. Phys. Lett. 719 (2019) 1–7.

[40] A. Ait hssi, E. Amaterz, N. labchir, L. Atourki, I.Y. Bouderbala, A. Elfanaoui, A. Benlhachemi, A. Ihlal, K. Bouabid, Electrodeposited ZnO nanorods as efficient photoanodes for the degradation of rhodamine B, Phys. Status Solidi. 217 (2020) 2000349.

[41] Y. Wang, J. Gao, X. Wang, L. Jin, L. Fang, M. Zhang, G. He, Z. Sun, Facile synthesis of core-shell ZnO/Cu 2 O heterojunction with enhanced visible light-driven photocatalytic performance, J. Sol-Gel Sci. Technol. 88 (2018) 172–180.

[42] C. Hsu, Y. Chuo, L. Hsu, Y. Pan, Y. Liu, UV and visible light induced photocatalytic degradation on p–n Cu2O/ZnO nanowires decorated with Au–Pd alloy nanoparticles, Adv. Mater. Interfaces. 6 (2019) 1801744.

[43] X. Wang, Y. Zhang, Q. Wang, B. Dong, Y. Wang, W. Feng, Photocatalytic activity of

Cu2O/ZnO nanocomposite for the decomposition of methyl orange under visible light irradiation, Sci. Eng. Compos. Mater. 26 (2019) 104–113.

[44] D. Malwal, P. Gopinath, Enhanced photocatalytic activity of hierarchical three dimensional metal oxide@ CuO nanostructures towards the degradation of Congo red dye under solar radiation, Catal. Sci. Technol. 6 (2016) 4458–4472.

[45] S. Shankar, M. Saroja, M. Venkatachalam, G. Parthasarathy, Photocatalytic degradation of methylene blue dye using ZnO thin films, Int. J. Chem. Concepts. 03 (2017) 180–188.

[46] M.J. Kadhim, M.A. Mahdi, J.J. Hassan, A.S. Al-Asadi, Photocatalytic activity and photoelectrochemical properties of Ag/ZnO core/shell nanorods under low-intensity white light irradiation, Nanotechnology. 32 (2021) 195706.

[47] W. Vallejo, A. Cantillo, B. Salazar, C. Diaz-Uribe, W. Ramos, E. Romero, M. Hurtado, Comparative Study of ZnO Thin Films Doped with Transition Metals (Cu and Co) for Methylene Blue Photodegradation under Visible Irradiation, Catalysts. 10 (2020) 528.

[48] F.A. Cataño, H. Gomez, E.A. Dalchiele, R.E. Marotti, Morphological and structural control of electrodeposited ZnO thin films and its influence on the photocatalytic degradation of methyl orange dye, Int. J. Electrochem. Sci. 9 (2014) 534–548.